Aalborg Universitet

SOGI-FLL error-and-hold algorithm for improving the response in face of voltage sags and swells with a small computational burden

Matas, J.; Golestan, S.; El Mariachet, J.; Abdali, S.; Al Hanaineh, W.; Guerrero, J. M.

Link to publication from Aalborg University

SOGI-FLL error-and-hold algorithm for improving the response in face of voltage sags and swells with a small computational burden

J. Matas [a], S. Golestan [b], J. El Mariachet [a], S. Abdali [a], W. Al Hanaineh [a,*], J.M. Guerrero [b]

[a] Electric Engineering Department, Polytechnic University of Catalonia (EEBE-UPC), Barcelona 08019, Spain
[b] Department of Energy Technology, Aalborg University, Aalborg 9200, Denmark

ARTICLE INFO

ABSTRACT

The Second Order Generalized Integrator–Frequency Locked Loop (SOGI-FLL) is a widely used and popular adaptive filter for estimating grid voltage parameters with minimal computational burden. However, it is vulnerable to voltage sag and swell faults, especially voltage sags that can significantly distort the estimated frequency. In this paper, we propose an error-and-hold algorithm for the SOGI-FLL that can quickly detect faults and hold the estimated frequency during these perturbations. The algorithm uses the absolute value of the SOGI's error, its average, and the average of the FLL's estimated frequency to operate. It reduces induced errors in the SOGI-FLL's quadrature outputs, improves the FLL's transient response, holds the estimated frequency, and restores the phase to its previous value before the fault. The proposed algorithm is a straightforward and low computational burden algorithm that can be executed on a low-cost processor. We validate the effectiveness of the proposed error-and-hold algorithm through simulations and experimental results.

1. Introduction

Distributed Generators (DGs) must synchronize with the utility grid to meet their power injection and quality requirements [1–4]. To this end, DGs must accurately estimate the amplitude voltage, frequency, and phase of the grid voltage in real-time. Various grid monitoring techniques can be employed to obtain estimates of these parameters and remain synchronized with the grid [5–28]. However, these estimates can be distorted by a range of network-related phenomena such as harmonics [7–10,12–20], DC-offset voltage [11–15], subharmonics [12], step frequency changes [7,9–10,12–20], unbalanced grid voltage [8–10,13], as well as more recently, voltage sags [16–20] and swells [18–19]. Such distortions can result in significant deviations from actual grid behavior and impact DG performance, leading to additional distortion in the grid and exacerbating grid problems [7–20]. Thus, fast, accurate, and less-distorted grid parameter estimates are essential to ensure good-quality DG operation under distorted grid conditions and prevent further distortion.

In recent years, the SOGI-FLL has gained popularity as a choice for estimating grid parameters due to its simple implementation and low computational requirements. It can be viewed as a second-order Band-Pass Filter (BPF) combined with a Frequency Locked Loop (FLL) that

adjusts the SOGI's center frequency to match the grid frequency [22].

The dynamic of the SOGI-FLL has been analyzed in previous studies [23,26,28], which have demonstrated that the structure can be vulnerable to distortions caused by various factors such as DC-offset voltage, harmonics, subharmonics, faults, voltage sags, and voltage swells. Specifically, research in [26] revealed that voltage sags have the greatest impact on the SOGI-FLL, causing high levels of peak distortion in the estimated frequency of the FLL response, while voltage swells have a similar but less significant impact.

According to the IEEE 1159 definition, voltage sags and swells are transient disturbances in the amplitude of the grid voltage, with durations ranging from 0.5 cycles to 1 min. Voltage sags are often caused by faults in the line due to short circuits, overloads, or the starting of large motors [2,4]. On the other hand, voltage swells can be caused by single line-to-ground faults or the de-energization of large loads, among other causes. The amplitude reduction due to voltage sags can range from 0.9 per unit (pu) to 0.1 pu, while voltage swells can cause the amplitude to increase from 1.1 pu to 1.8 pu.

In [18], an adaptive approach based on a Finite State Machine (FSM) algorithm is proposed to mitigate the impact of voltage sags and swells on the FLL by modifying the gains of the SOGI-FLL. However, this method involves a set of linear and nonlinear equations to calculate the

---

* Corresponding author.
E-mail address: wael.hasan.ahmad.al.hanaineh@upc.edu (W. Al Hanaineh).

SOGI-FLL gains, making it challenging to implement. Additionally, the adjustment of SOGI-FLL gains is based on the depth of the voltage sags, which must be measured, resulting in a reduction of the magnitude, size, and duration of the frequency estimated by the FLL. Moreover, the FSM has a slow response, which limits the performance improvement.

In [19], a more effective approach has been proposed, using the SOGI's error signal as well as its absolute and averaged values to operate. This approach enables a faster response to perturbations in the voltage by directly monitoring the error and its average signals. The average error signal is compared to two thresholds: one used to detect the beginning of the perturbation and trigger the algorithm, and the other for determining when the perturbation ends. The threshold used to detect the beginning of the perturbation is also designed to enable the SOGI-FLL to respond to ± 2 Hz step changes in the grid frequency, including a possible harmonic distortion of 3%.

In [19], the algorithm only requires two states, constant gains, and does not depend on measuring the depth or height of voltage sag or swell. It also does not need to identify whether the perturbation is a voltage sag or swell. As a result, it is easier to implement compared to the approach reported in [18].

In this paper, we present a modified error-based algorithm that freezes the frequency estimate of the SOGI-FLL during voltage sag or swell perturbations. To achieve this, the FLL gain is set to zero when the perturbation is detected, and the frequency is set to the FLL frequency obtained at previous instants before the perturbation event.

In this algorithm, we introduce a new Low-Pass Filter (LPF) in the scheme with a very low cutoff frequency that has a slow transient response regarding the dynamic response of the FLL. As a result, when the perturbation is detected, the LPF still holds a value close to the previous frequency estimate value before the perturbation. The algorithm reads this value, places it in an internal memory, and uses it to provide the frozen frequency during the perturbation. This minimizes the distortions in the SOGI outputs created by the perturbation, improves the behavior of the voltage amplitude estimate, and reduces the SOGI-FLL transient duration. Additionally, using the memorized frozen frequency, the phase of the SOGI-FLL can be digitally reconstructed using a discrete integrator with a reset that can be controlled by the FSM algorithm.

As a result, from the perspective of the DG, the grid frequency will remain frozen and the phase will be reconstructed during the voltage sag or swell perturbation, which can keep the DG synchronized with the frequency and phase that the grid had just in the moments before the perturbation, avoiding further disturbance of the grid.

When the transient distortion affecting the SOGI-FLL disappears, the algorithm returns to providing the real frequency estimate of the FLL, and the SOGI-FLL returns to normal operation. We provide simulations and experimental results to demonstrate the feasibility of the proposed algorithm.

The rest of this paper is organized as follows. Section II provides a detailed and comprehensive analysis of the behavior of the SOGI-FLL structure, particularly in detecting and responding to voltage sags and swells. Our analysis builds upon and improves upon the analysis presented in [19]. Section III describes the proposed algorithm in detail, explaining how it improves the performance of the SOGI-FLL during voltage sag or swell perturbations. Finally, Sections IV and V present the simulation and experimental results, respectively, which demonstrate the feasibility and effectiveness of the proposed algorithm.

2. SOGI-FLL response to voltage sags and swells

Fig. 1 shows the structure of the SOGI-FLL, where v_g represents the grid voltage, ω_o represents the center frequency, and v_α and v_β represent in-phase and quadrature-phase outputs of the SOGI filter, respectively. The FLL functions as a gradient descent estimator [7,21], and provides an estimate of the grid frequency, denoted as ω. This frequency estimate is used to adapt the center frequency of the SOGI filter to grid frequency
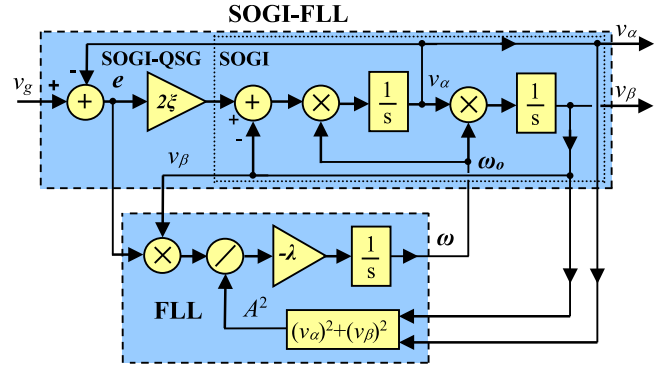

Fig. 1. Block diagram of the SOGI-FLL.

changes, such that, $\omega_o = \omega$.

The SOGI-FLL has a BPF-like behavior for its α-axis output signal, v_α, and an LPF-like behavior for its β-axis output signal, v_β, as described in [21]. The transfer functions for these behaviors can be derived by considering ω_o as a constant and are given as follows:

$$H_\alpha(s) = \frac{v_\alpha(s)}{v_g(s)} = \frac{2\xi\omega_o \bullet s}{s^2 + 2\xi\omega_o \bullet s + \omega_o^2}, \quad (1)$$

$$H_\beta(s) = \frac{v_\beta(s)}{v_g(s)} = \frac{2\xi\omega_o^2}{s^2 + 2\xi\omega_o \bullet s + \omega_o^2}. \quad (2)$$

The differential equation that governs the behavior of the FLL is given by.

$$\frac{d\omega}{dt} = -\frac{\lambda}{A^2}e.v_\beta, \quad (3)$$

where A represents the estimated amplitude voltage of the grid, which is obtained by utilizing the SOGI filter outputs as follows:

$$A = \sqrt{v_\alpha^2 + v_\beta^2}. \quad (4)$$

The small-signal model of the SOGI-FLL can be obtained by assuming a quasi-locked operating point for amplitude voltage, frequency, and phase [22,24,26]. This model is described by equations (5) and (6) and is shown in Fig. 2.

$$\frac{A(s)}{A_g(s)} \cong \frac{\xi\omega_n}{s + \xi\omega_n}, \quad (5)$$

$$\frac{\omega(s)}{\omega_g(s)} \cong \frac{\lambda/2}{s^2 + \xi\omega_n \bullet s + \lambda/2}, \quad (6)$$

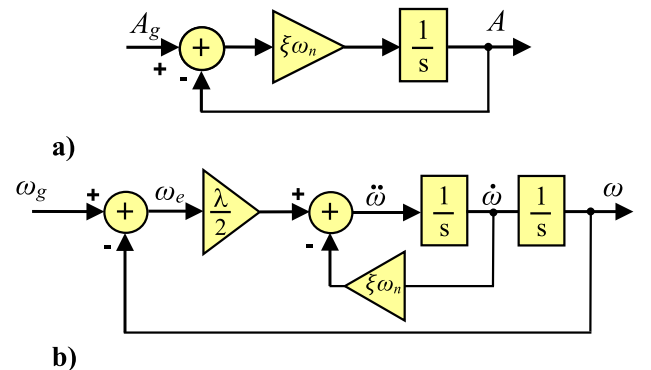In the above equations, ω_g and A_g are the grid frequency and

Fig. 2. Linearized model of the SOGI-FLL. a) Estimated amplitude voltage. b) Estimated frequency.
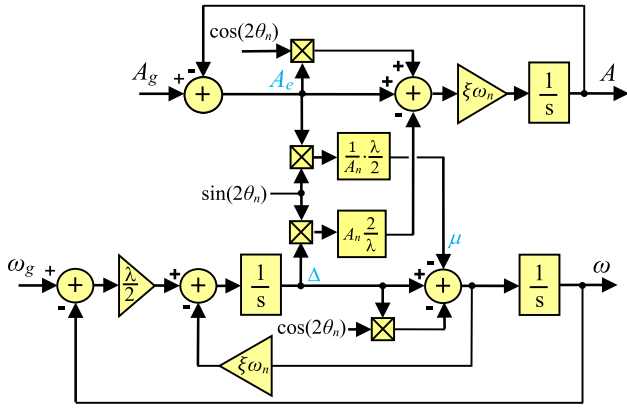
Fig. 3. LTP model of the SOGI-FLL showing cross-terms between its amplitude and frequency estimation loops.

amplitude voltage, respectively; $\omega_n = 2\pi 50$ rad/s is the nominal value of the grid frequency; and A and ω denote small perturbations in the estimated frequency and amplitude voltage, respectively.

The small-signal models presented in (5) and (6) allow to express the transient response of the estimates A and ω in the event of a sudden change in A_g and ω_g, respectively, for a given value of ξ and λ.

The model presented in (5) describes a first-order system, and according to control theory, its response to a step change in A_g is a first-order exponential transient without overshoot, with a time constant $\tau = 1/\xi\omega_n$.

On the other hand, the model presented in (6) corresponds to a second-order system, and its transient response is determined by the roots of its characteristic polynomial, which is expressed as follows:

$$s^2 + \xi\omega_n \bullet s + \lambda/2 = 0. \tag{7}$$

In (7), it can be seen that $\xi\omega_n$ and $\lambda/2$ are related to the damping factor, ξ', and the natural undamped frequency, ω', respectively, as defined in the standard form of a second-order system, which is given as $s^2 + 2\xi'\omega' \bullet s + (\omega')^2 = 0$. By setting $\xi\omega_n = 2\xi'\omega'$ and $\lambda/2 = (\omega')^2$, it can be observed that:

$$\lambda = 2(\omega')^2, \tag{8}$$

$$\omega' = \frac{\xi\omega_n}{2\xi'}, \tag{9}$$

Substituting (9) into (8) leads to.

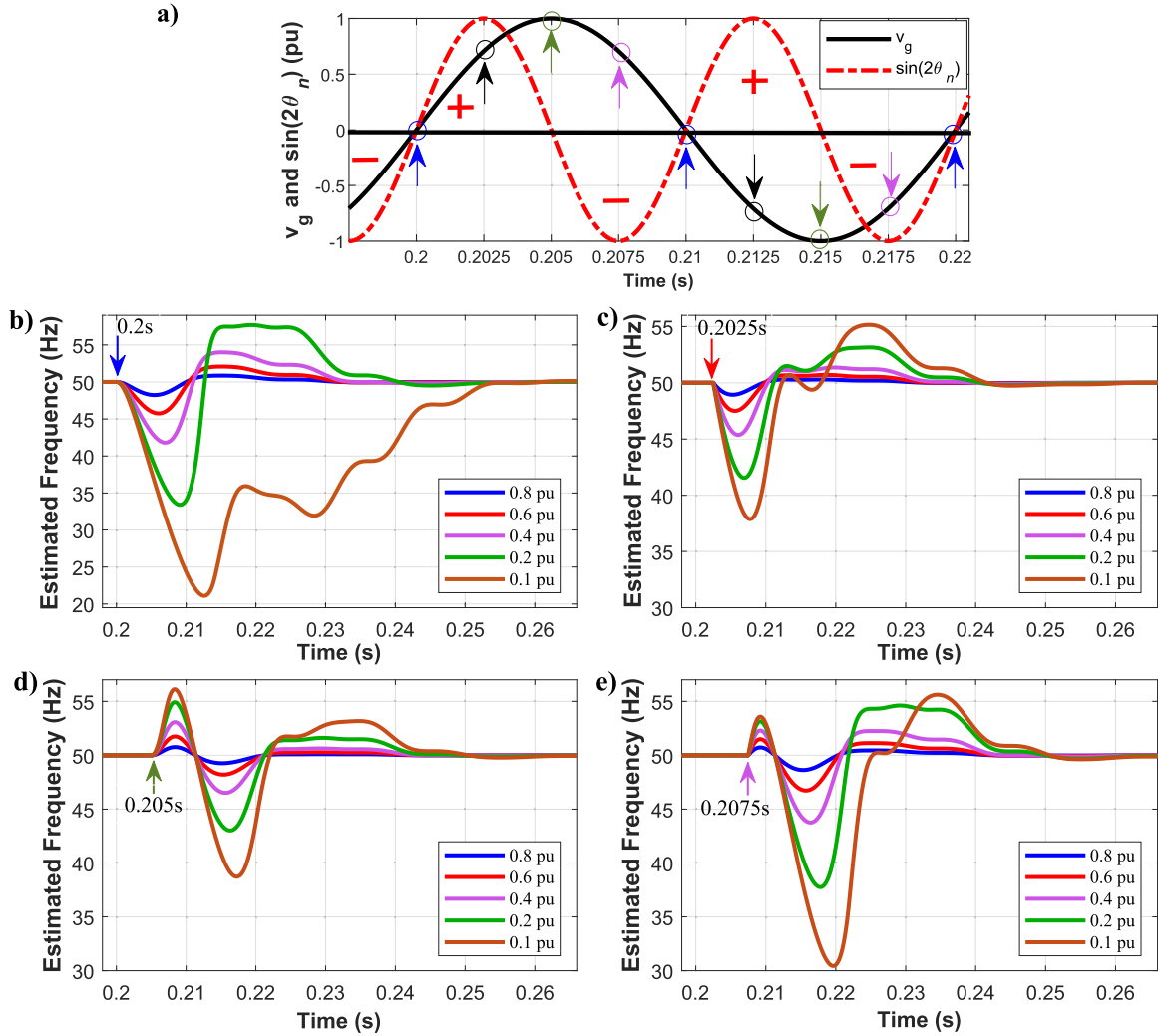**Fig. 4.** Spurious transients in the estimated frequency of the SOGI-FLL for varying depths of voltage sags (ranging from 0.8 pu to 0.1 pu) and at different moments within a half grid period. a) Grid voltage, $sin(2\theta_n)$ term, and moments in which the faults happen; b) for voltage sags at t = 0.2 s; c) for voltage sags at t = 0.202 5 s; d) for voltage sags at t = 0.2050 s; e) for voltage sags at t = 0.2075 s.

$$\lambda = \frac{\xi^2 \omega_n^2}{2\xi^{'2}}, \tag{10}$$

Choosing $\xi^{'} = \xi = 1/\sqrt{2}$ as suggested in the literature to achieve an optimum tradeoff between overshoot, M_p, and settling time, t_s, leads to:

$$\lambda = \lambda_N = 0.5\omega_n^2. \tag{11}$$

where λ_N represents the nominal value of the FLL's gain used here. Substituting these values of ξ and λ, in (7) yields the roots of the characteristic polynomial as $s_{1,2} = -111.07 \pm 111.07j$ resulting in a second-order transient response characterized by a maximum overshoot of $M_p = 4.32\%$ and $t_s = 36$ ms.

Under a voltage sag, the estimated amplitude A by the SOGI-FLL may exhibit small nonlinearities, but it closely follows the first-order transient response predicted by the model in (5). On the other hand, the frequency estimation loop shows significant spurious transients during voltage sags, with frequency peak values that increase proportionally with the depth level of the voltage sag. In the worst-case scenario of a 0.1 pu sag, the frequency peak can reach up to 29 Hz, causing considerable errors at the v_α and v_β outputs and introducing significant distortion into the system.

The LTI model in Fig. 2 does not predict this behavior as it ignores the couplings that are excited between the amplitude and frequency estimation loops of the SOGI-FLL. These couplings are evident in Fig. 3, which shows a linear time-periodic (LTP) model of the SOGI-FLL [26,28]. The LTP model reveals that the estimated ω is directly perturbed by the error of the amplitude voltage estimate multiplied by $\lambda/(2A_n)$ and $\sin(2\theta_n)$, while the estimate A is perturbed by the integral of the frequency error minus a frequency derivative term, all multiplied by $2A_n/\lambda$ and $\sin(2\theta_n)$. θ_n and A_n are the nominal phase and amplitude voltages of the grid.

The dynamics designed by (11) lead to the fact that $\lambda \gg A_n$, where the specific values are $\lambda = 49348$ and $A_n = 310.2$. So, looking at the LTP model of Fig. 3, it can be seen that the cross-term gains between the amplitude and frequency estimation loops satisfy the following relationship:

$$\frac{1}{A_n} \cdot \frac{\lambda}{2} \gg A_n \frac{2}{\lambda}, \tag{12}$$

i.e., putting numbers $\lambda/(2A_n) = 79.3$ and $2A_n/\lambda = 0.0126$. Therefore, it can be inferred that the amplitude estimation loop, with a gain of 79.3, can cause a much larger perturbation in ω than the frequency estimation loop can have on A, with a gain of 0.0126.

Then, considering the frequency loop, this loop usually could be affected by perturbations in the grid frequency or phase. These perturbations will be affected by the integral of the error, and as a result, the distortion Δ induced in this loop will perturb the upper amplitude loop of Fig. 3, with a small cross-gain. On the other hand, in the case of the amplitude loop, this loop will be directly affected by a voltage sags or swells. Consequently, any sag will significantly impact the bottom frequency loop with a strong cross-gain term. This explains why voltage sags highly impact the estimated frequency of the SOGI-FLL.

In addition, the term $\sin(2\theta_n)$ in Fig. 3 introduces a gain-modulating effect that can either amplify or reduce the magnitude of perturbation in ω and A, depending on the occurrence of faults in the $2\theta_n$ phase, as shown in Fig. 4. This term also has the capability to change the sign of the perturbation, resulting in a periodic perturbation phenomenon at every half-cycle of the grid. Note that $2\theta_n$ represents a double frequency component, since $\theta_n = \omega_n t$. Moreover, this phenomenon occurs for all faults happening at the same phase instants within a grid voltage period. For instance, for a 0.1pu voltage sag, the error in the amplitude loop of Fig. 3 reaches a maximum peak of.

$$A_e = A_g - A = 0.1A - A = -0.9pu$$

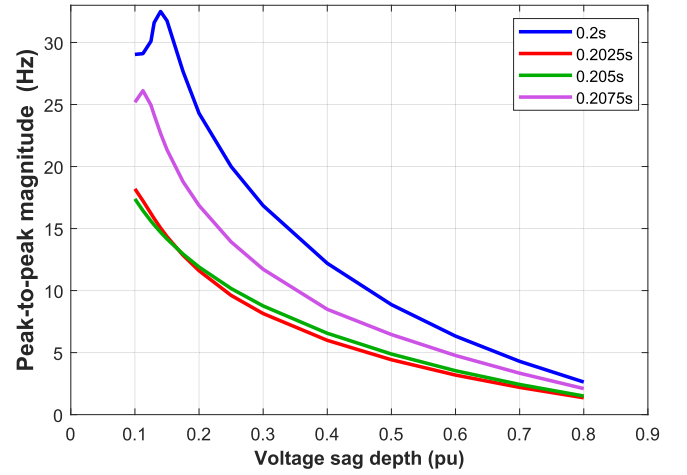So, this perturbation will affect the frequency loop modulated by the

Fig. 5. Peak-to-peak magnitude of the perturbation induced by the voltage sag's depth in Fig. 4.

sinusoidal term as:

$$\mu = A_e . sin(2\theta_n).79.3 \tag{13}$$

In Fig. 4.a, it could be seen the modulation effect of the $sin(2\theta_n)$ term when a voltage sag happens in a given moment and last for some time. The impact of $sin(2\theta_n)$ can be observed to have a positive sign at 0.2025 s and 0.2125 s, while it exhibits a negative sign at 0.2075 s and 0.2175 s. Additionally, it is zero at 0.2 s, 0.205 s, 0.21 s, 0.215 s, and 0.22 s.

Regarding the duration of the transient induced by the sag on A_e, the term $sin(2\theta_n)$ modulates in time the perturbation in the frequency loop over time. For instance, if the sag happens at 0.2 s and lasts for multiple periods, $sin(2\theta_n)$ will change the sign four times within the first period alone. This effect can be seen in general in Fig. 4.b, 4.c, 4.d, and 4.e, where decreasing oscillations are evident over time.

Overall, it can be concluded that the induced perturbation on the frequency loop by a voltage sag is significant and exhibits nonlinearity, with a repetitive pattern every half-period of the grid voltage. However, the magnitude of the perturbations cannot be precisely estimated as they are affected by the size of large-signal perturbations, as noted in [28].

To assess the actual impact of voltage sags on ω, a series of simulations are conducted and presented in Fig. 4. These simulations were performed using optimal gains, i.e., $\xi = 0.707$ and $\lambda = 0.5\omega_n^2$, and involved various voltage sag depths ranging from 0.8 pu to 0.1 pu. Four different time instances within a half-period of the grid in which a fault could potentially occur ($t = 0.2, 0.2025, 0.205,$ and 0.2072 s) are considered to demonstrate the effect of the $sin(2\theta_n)$ term in the LTP model. The simulations are limited to a half-period as the perturbations within each half-period are identical for every half-period of the grid voltage at the same points on the sinusoidal waveform, see Fig. 4.a. For example, the perturbation induced at $t = 0.2$ s would also occur at $t = 0.21$ s, and so on (as shown by the colored arrows in Fig. 4a, which indicate the moment of sag occurrence).

Fig. 5 shows the measured peak-to-peak magnitude of spurious transients in the estimated frequency as a function of the voltage sag depth. The plot reveals that the magnitude of transients increases non-linearly with the depth level of the voltage sag. In the worst cases, the magnitude of frequency transients reaches 32.5 Hz and 26.11 Hz for voltage sags at $t = 0.2$ s and $t = 0.2075$ s, with depths of 0.14 pu and 0.13 pu, respectively.

A series of simulations has also been carried out to assess the actual impact of voltage swells (ranging from 1.2 pu to 1.8 pu) on ω.

These simulations revealed a similar perturbation phenomenon to that observed in Fig. 4. However, in comparison to voltage sags, the impact of voltage swells on ω was found to be smaller, with peak-to-peak magnitudes of up to 6 Hz in the worst cases. This reduced impact is
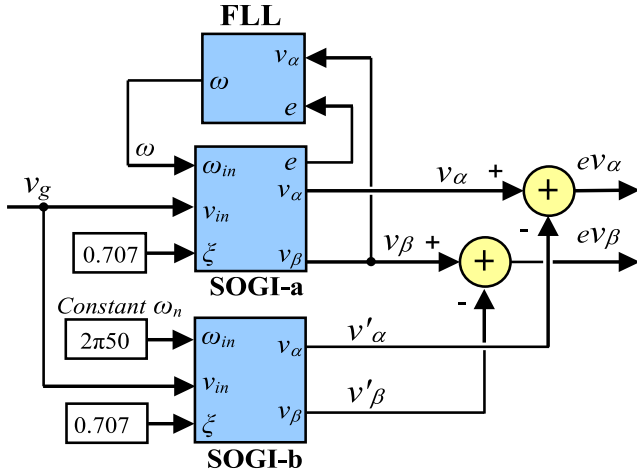
Fig. 6. Structure comparison for assessing the errors induced by voltage sags at the outputs of the SOGI-FLL filter.
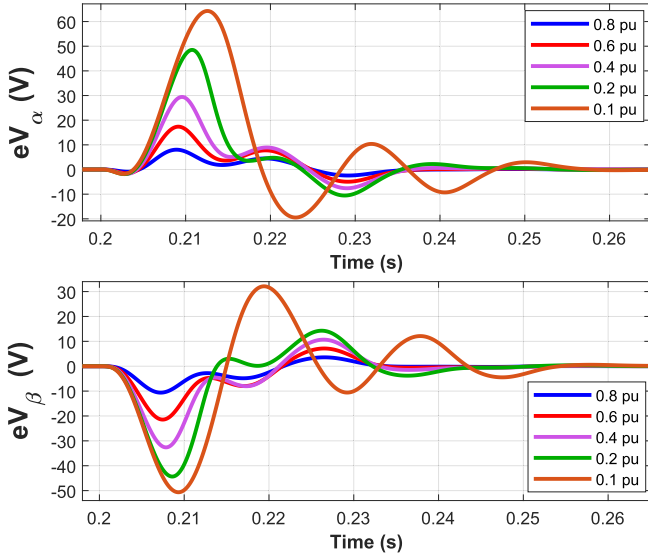

Fig. 7. Induced errors on the outputs of the SOGI filter, v_α and v_β, due to the impact of voltage sags with different depth sizes.

mainly attributable to the amplitude normalization (the division by A^2) in the FLL's governing nonlinear differential equation [see (3)]. Note that this division reduces the FLL gain during voltage swells. As a result, smaller spurious transients in the FLL output are observed during voltage swells than during voltage sags.

Spurious frequency transients induced by voltage sags and swells may cause noticeable errors in the outputs of the SOGI filter, v_d and v_q. To assess these errors, the v_α and v_β outputs of a SOGI-FLL (depicted in Fig. 6) are compared with those of an identical SOGI (depicted as SOGI-b), operating at a fixed nominal frequency.

Fig. 7 shows the magnitude of errors in the outputs of the SOGI filter caused by the same voltage sags simulated in Fig. 4(b) at $t = 0.2s$. It can be observed that the peak-to-peak values of the errors reach 83.7 V and 82.8 V for $ev_\alpha = v_\alpha - v'_\alpha$ and $ev_\beta = v_\beta - v'_\beta$, respectively, which corresponds to 27% and 26.7% of A_n, respectively. The assessment has also been conducted for voltage swells, which can result in errors of up to 37 V for ev_α and 57 V for ev_β, corresponding to 11.9% and 18.3% of A_n, respectively. These results confirm that voltage sags and swells have a substantial impact on the performance of the SOGI-FLL.
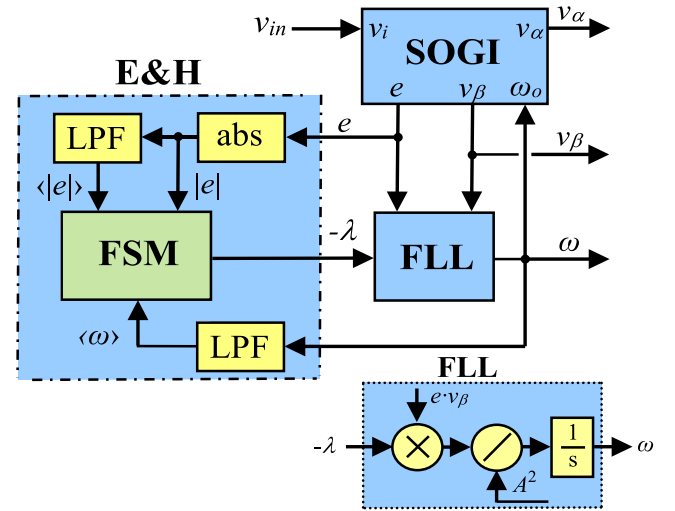

Fig. 8. Error & hold algorithm scheme proposal for the SOGI-FLL.

3. Error & hold algorithm for reducing the perturbation impact in the SOGI

The spurious frequency transients caused by voltage sags and swells can be effectively mitigated by utilizing the error signal of the SOGI, i.e., $e = v_g - v_\alpha$. This is because the fault impact is directly received by the SOGI through this error. The proposed algorithm, named SOGI-FLL "Error & Hold" (SOGI-FLL-E&H), utilizes the error signal, $|e|$, and a low-pass filtering of $|e|$ and ω to obtain their average values, $\langle|e|\rangle$ and $\langle\omega\rangle$, respectively, to operate, as shown in the schematic diagram in Fig. 8. The E&H algorithm uses an FSM that needs only two states: S1 for "normal" operation and S2 for "faulted" operation. Fig. 10 depicts the state diagram of the FSM and part of the Matlab code used for implementation.

In the E&H algorithm, during a fault, the FLL gain λ is set to zero and the estimated frequency, ω, is frozen at its value prior to the fault, which is denoted as ω_-. The frequency ω_- is obtained by applying an LPF to the estimated frequency, $\omega_- = LPF(\omega)$. To reconstruct the phase of the grid voltage, the algorithm uses the memorized frequency ω_- and a discrete integrator with the sampling time T_s.

In Fig. 8, the LPF for achieving the average frequency has been designed to satisfy two conditions simultaneously: filtering potential harmonics in the grid voltage and serving as an analog memory to provide ω_-. This is accomplished due to the inherent delay introduced by the LPF, which is determined by its cutoff frequency $\omega_{c\_\omega av}$. In this sense, the value of $\omega_{c\_\omega av}$, shown at Table 1, has been deliberately chosen to be very low compared with the frequency range of the harmonics. Consequently, prior to a voltage sag, this LPF provides a stable and flat averaged of the estimated frequency, denoted as $\langle\omega\rangle$ in Fig. 8. This average remains constant and serves as the reference for the E&H

Table 1
SOGI-FLL-E&H parameters responding to voltage sags and swells.

Parameter	State	
	S1	S2
ξ	0.707	0.707
λ	$0.5\omega_n^2$	0

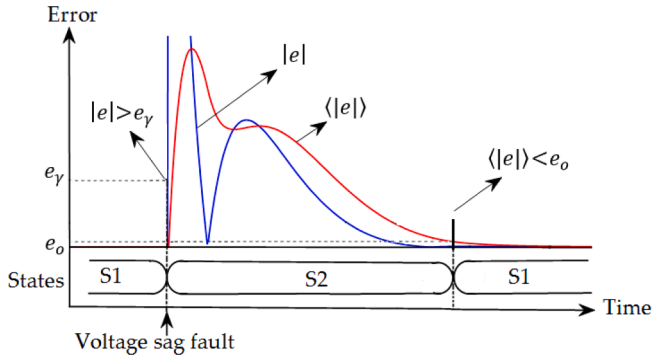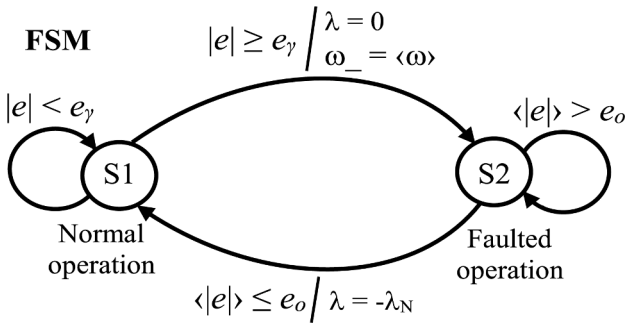| Parameter	Value
e_γ	23 V
e_o	4 V
$\omega_{c\_eav}\omega_{c\_\omega av}$	$2\pi10$ rad/s
	2π rad/s

Fig. 9. An example of the behavior of $|e|$ and $\langle|e|\rangle$ during a voltage sag with the proposed SOGI-FLL-E&H.


```
% Initialization
St = S1;        %Set initial state
λ = -λ_N;       %Set operating lambda gain

if (St = S1)
    if (abs_error ≥ e_γ)
        St = S2;        %change to state S2
        ω_ = ⟨ω⟩;       %read averaged frequency
        λ = 0;          %freeze λ
    end
else
    if (avg_error ≤ e_o)
        St = S1;        %change to state S1
        λ = -λ_N;       %provide nominal lambda
    end
```

Fig. 10. Finite state machine diagram using two states and Matlab code.

algorithm when it is triggered by a voltage sag. Therefore, the algorithm remains unaffected by harmonics in this regard. In addition, the LPF filters out the undesirable effects of transient noise in ω.

On the other hand, and at the same time, the LPF's low cutoff frequency leads to a very slow transient response. Then, when the E&H algorithm is triggered, the LPF provides a value that is very close to the previous existing one at the sag. This value is read by the algorithm at the beginning and stored in the internal variable ω_-. Throughout S2, this stored value is used to ensure stability and continuity in the estimated frequency provided by the algorithm.

During a fault such as a voltage sag, the absolute value of the error signal ($|e|$) exhibits a sharp-impulsive transient response because it is equal to the difference between the grid voltage (v_g) and the estimated voltage (v_α), i.e., $|e| = |v_g - v_\alpha|$. This behavior is shown in Fig. 9, which illustrates an example of $|e|$ and $\langle|e|\rangle$ during a voltage sag. To detect a fault, the algorithm compares $|e|$ to a given threshold e_γ. If $|e|$ exceeds e_γ,

the algorithm reads the output of the LPF and stores it in the internal variable memory ω_-. The algorithm then switches from state S1 to S2 and sets λ to zero, freezing ω, see Fig. 10. The threshold e_γ is designed to enable the algorithm to respond to a frequency step change of ± 2 Hz while also allowing for the passage of a 3rd harmonic with a 3% amplitude voltage regarding nominal.

To transition from state S2 to S1, the algorithm compares the average value of the error signal, $\langle|e|\rangle$ (shown in red in Fig. 9), with a given threshold e_o. This threshold indicates when spurious frequency transients have dampened. Note that $\langle|e|\rangle$ is obtained by filtering $|e|$ with other LPF with a suitable cutoff frequency, ω_{c_eav}. The threshold e_o has been designed through a trial-and-error process to cover all possible voltage sag/swell moments, depths, and heights considered in the study. Once the condition $\langle|e|\rangle < e_o$ is met, the algorithm initiates the transition to normal operation, Fig. 10. The selected value for e_o, as shown at Table 1, has been checked to ensure a smooth transition from state S2 to S1, minimizing the duration of the transients induced by the voltage sags and swells.

In summary, the proposed algorithm maintains a stable frequency during voltage sags/swells by freezing it at the same level as before the fault and reconstructs the phase using a memorized value of ω_-. This ensures that the frequency and phase remain stable during voltages sags/swells, which is beneficial for applications like wind turbines that need to stay connected to the grid during faults. Both LPFs used in the algorithm, Fig. 8, are chosen to be of single-order type for simplicity of implementation. Note in Fig. 8 that a block diagram detailing a part of the internal implementation of the FLL is shown below the E&H algorithm. This is because it represents a small change from the initial FLL scheme depicted in Fig. 1.

In summary, the proposed algorithm maintains a stable frequency during voltage sags/swells by freezing it at the same level as before the fault and reconstructs the phase using a memorized value of ω_-. This ensures that the frequency and phase remain stable during voltages sags/swells, which is beneficial for applications like wind turbines that need to stay connected to the grid during faults. Both LPFs used in the algorithm, Fig. 8, are chosen to be of single-order type for simplicity of implementation. Note in Fig. 8 that a block diagram detailing a part of the internal implementation of the FLL is shown below the E&H algorithm. This is because it represents a small change from the initial FLL scheme depicted in Fig. 1.

4. Simulations and experimental results

The proposed SOGI-FLL-E&H scheme shown in Fig. 8 has been implemented using Matlab/Simulink software and its performance has been evaluated through simulations and experiments. The gains of the SOGI-FLL-E&H during S1 and S2, along with the values of the thresholds, e_γ and e_o, and cutoff frequencies, $\omega_{c\_\omega av}$ and ω_{c_eav}, are listed in Table 1.

The threshold e_γ plays a critical role since triggers the algorithm. e_γ has been designed to allow the passage of a 2 Hz frequency step perturbation, including a 3rd of harmonic distortion of 3% amplitude, during normal operation of the SOGI-FLL in an attempt of making the algorithm more general. The choice has been made considering the ± 1 Hz frequency maximum allowable range operation for the European grid network. This means that if the grid frequency is at 49 Hz, the algorithm could face a frequency step change from 49 Hz to 51 Hz. Similarly, if the grid frequency is at 51 Hz, there could be a step change from 51 Hz to 49 Hz.

The value of e_γ has been chosen by directly measuring the maximum peak value in the transient response of $|e|$, simulated using Matlab/Simulink. The measured peak value was of 21.7 V, and e_γ has been placed at 23 V, which is slightly above the peak.

Nevertheless, an alternative design could be made by knowing that the error signal of the SOGI filter has the following Notch Filter (NF)
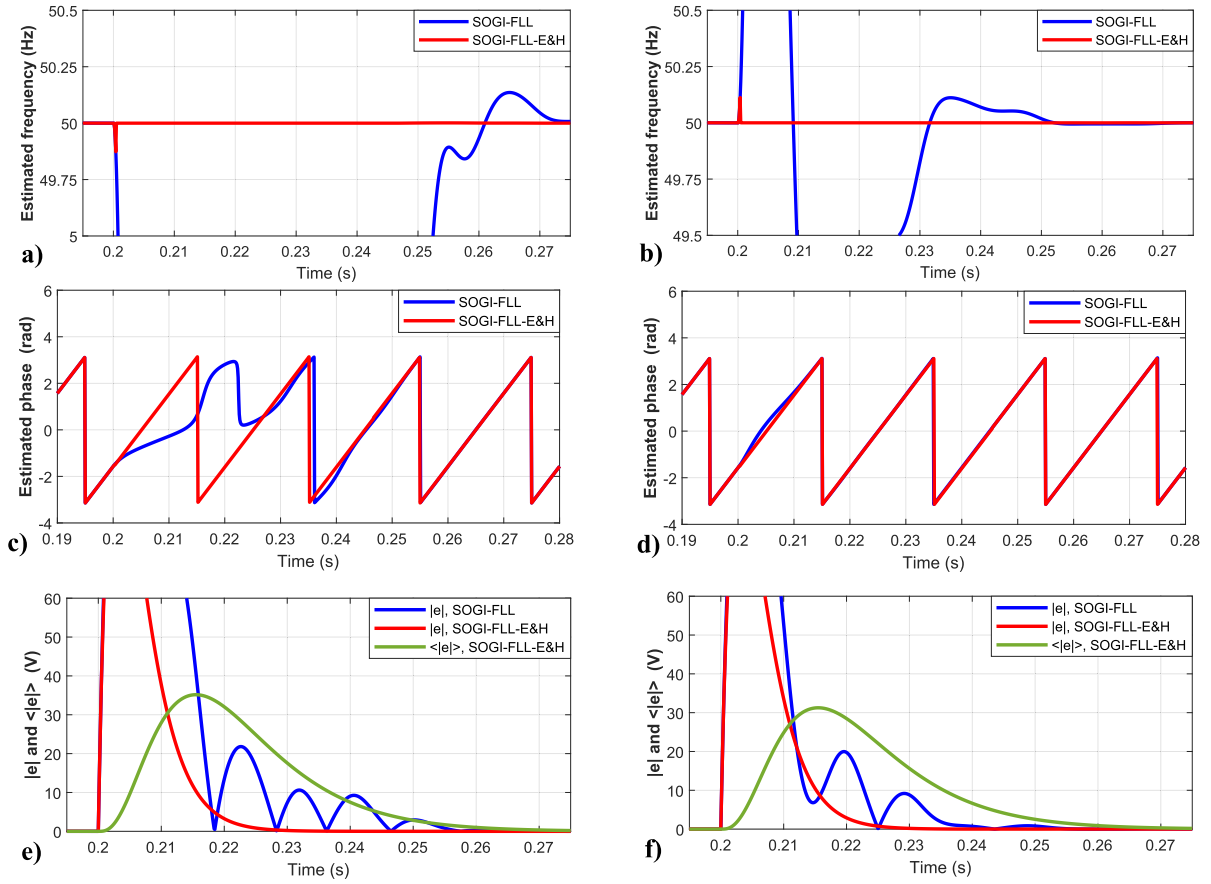
Fig. 11. SOGI-FLL and SOGI-FLL-E&H estimated frequency, phase, and error transient responses to a 0.1 pu voltage sag and 1.8 pu voltage swell happening at 0.2 s. a) and b) Estimated frequency; c) and d) Estimated phase; e) and f) $|e|$ and $\langle|e|\rangle$; a), c) and e) are for the voltage sag; b), d) and f) are for the voltage swell.

transfer function with respect to the input:

$$H_e(s) = \frac{e(s)}{v_g(s)} = \frac{s^2 + \omega_o^2}{s^2 + 2\xi\omega_o \bullet s + \omega_o^2}. \tag{14}$$

Considering that the grid is at $\omega_n = 2\pi 50$, the FLL is tuned ($\omega_o \cong \omega_n$), and a sudden 2 Hz frequency step perturbation happens, the SOGI instantly becomes untuned and the error increases from zero to the following maximum value:

$$|e|_{peak} = |v_g|.|H_e(j\omega)|_{\omega=\omega_g=2\pi 52} \tag{15}$$

That is, because the SOGI-FLL is untuned, the NF behavior of the error attenuates the input. By knowing that $|v_g| = A_n = 310.2V$ and, using the bode plot, $|H_e(j\omega)|$ at $\omega = 2\pi 52$ is $-26.3dB$, the peak error is calculated to be $|e|_{peak} = 15.01V$. Therefore, setting e_γ slightly above $|e|_{peak}$ is sufficient to handle the frequency perturbation. In this case, the threshold could be chosen as $e_\gamma = 17$. However, in this work, the effect of the 3rd harmonic distortion should be also included in (15). Thus, (15) becomes:

$$|e|_{peak} = |v_g||H_e(j\omega)|_{\omega=2\pi 52} + A_3|H_e(j\omega)|_{\omega=3.2\pi 52} \tag{16}$$

where A_3 is the amplitude voltage of the 3rd harmonic. So, taking into account that the 3% harmonic amplitude is $A_3 = 0.03A_n$ and $|H_e(j\omega)|$ at $\omega = 3.2\pi 52$ is $-2.1dB$, it results in $|e|_{peak} = 22.31V$. Then, the selected threshold, $e_\gamma = 23$, is slightly higher than the peak value.

In the discretization process, a third-order Adam–Bashforth method has been adopted to discretize the SOGI filter, following the discretization analysis performed in [27]. This method ensures an exact $-90°$ phase delay at the quadrature output of the SOGI filter and avoids the drawbacks associated with Backward, Forward and Tusting

discretization methods, especially for low sampling frequencies. The Adam–Bashforth discretization method is expressed as follows:

$$\frac{1}{s} \leftrightarrow \frac{T_s}{12} \frac{5z^{-3} - 16z^{-2} + 23z^{-1}}{1 - z^1}. \tag{17}$$

Meanwhile, the FLL's integrator and the LPFs used in Fig. 8 have been discretized using a Backward Euler method:

$$\frac{1}{s} \leftrightarrow \frac{T_s}{1 - z^1}, \tag{18}$$

since the FLL and LPFs do not exhibit the problems reported for the SOGI an allow for a simplified implementation.

The sample time, Ts, is set to 100 μs, which corresponds to a 10 kHz sample frequency. The LPF for achieving the averages of ω and $|e|$ has been also digitally implemented with a Backward Euler method. The integrators of these LPFs, when returning back to S1, have been reset to ω_- and 0, respectively.

Fig. 11 depicts the obtained results for the SOGI-FLL and SOGI-FLL-E&H for a $0.1pu$ voltage sag and for a $1.8pu$ voltage swell perturbations occurring at $0.2s$ when the grid is at zero voltage. Fig. 11.a, 11.c and 11.e correspond to the voltage sag, while Fig. 11.b, 11.d, and 11.f correspond to the voltage swell.

Note in the frequency response, Fig. 11.a and 11.b, that there is a small spurious peak in the SOGI-FLL-E&H, occurring precisely at 0.2 s, particularly because the fault happens at zero grid voltage. This small peak is due to that the error is momentarily zero at the fault, and grows by its own pace till it surpasses the threshold e_γ, which is the starting point to trigger the algorithm. Then, the spurious peak corresponds to the real perturbed estimate, which is almost instantly replaced by the memorized ω_- value, providing a frozen value till the end of the
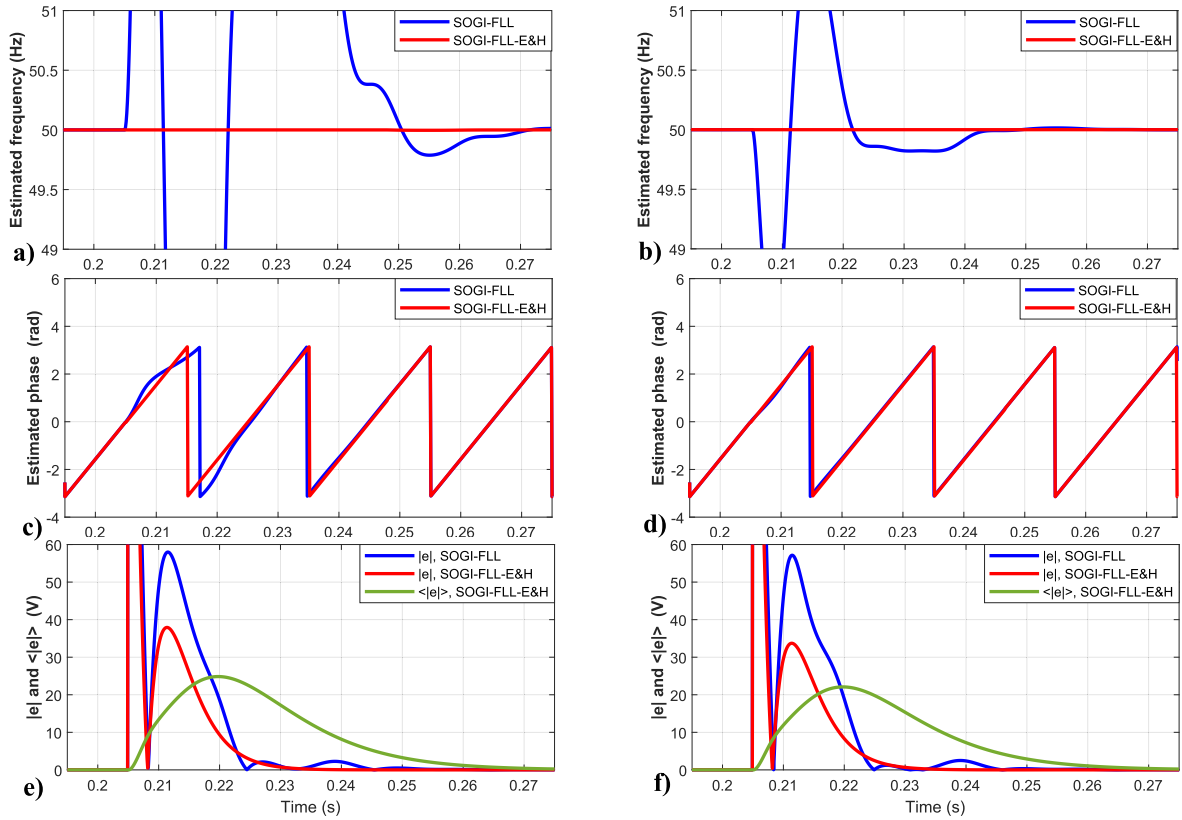
Fig. 12. SOGI-FLL and SOGI-FLL-E&H estimated frequency, phase, and error transient responses to 0.1 *pu* voltage sag and 1.8 *pu* voltage swell happening at 0.205 s. a) and b) Estimated frequency; c) and d) Estimated phase; e) and f) |*e*| and ⟨|*e*|⟩; a), c) and e) are for voltage sag; b), d) and f) are for voltage swell.

perturbation. This is only possible for faults that occur when the grid voltage is at zero, or very close to zero, i.e. below the defined threshold e_γ. Notice for the phase, Fig. 11.c and 11.d, how the phase is distorted in the SOGI-FLL, but reconstructed for the SOGI-FLL-E&H. Also, in Fig. 11. e, note that the perturbation lasts about 3 cycles for the SOGI-FLL, while it last about 1.5 cycles for the SOGI-FLL-E&H. A similar reduction in the time response can be observed for voltage swells, (Fig. 11.f), despite the fact that swells induce less perturbation.

In a similar way, Fig. 12 shows the SOGI-FLL and SOGI-FLL-E&H transient responses for a 0.1*pu* voltage sag and a 1.8*pu* voltage swell, happening at $t = 0.205s$, when the grid voltage is at its maximum level. Regarding the estimated frequency, note in this case that there is no spike produced at the frozen frequency responses. Regarding the phase, note that the phases had been reconstructed during the fault. Regarding the transient duration, note that for the SOGI-FLL, the transient lasts about 2.5 cycles, whereas is about 1.25 cycles for the SOGI-FLL-E&H.

Notice for the phase, Fig. 11.c and 11.d, how the phase is distorted in the SOGI-FLL, but reconstructed for the SOGI-FLL-E&H. Also, in Fig. 11. e, note that the perturbation lasts about 3 cycles for the SOGI-FLL, while it last about 1.5 cycles for the SOGI-FLL-E&H. A similar reduction in the time response can be observed for voltage swells, (Fig. 11.f), despite the fact that swells induce less perturbation.

In a similar way, Fig. 12 shows the SOGI-FLL and SOGI-FLL-E&H transient responses for a 0.1*pu* voltage sag and a 1.8*pu* voltage swell, happening at $t = 0.205s$, when the grid, voltage is at its maximum level. Regarding the estimated frequency, note in this case that there is no spike produced at the frozen frequency responses. Regarding the phase, note that the phases had been reconstructed during the fault. Regarding the transient duration, note that for the SOGI-FLL, the transient lasts about 2.5 cycles, whereas is about 1.25 cycles for the SOGI-FLL-E&H.

The value chosen for the threshold e_γ has been designed to be able to accommodate a frequency step change of ±2Hz and including a 3% THD
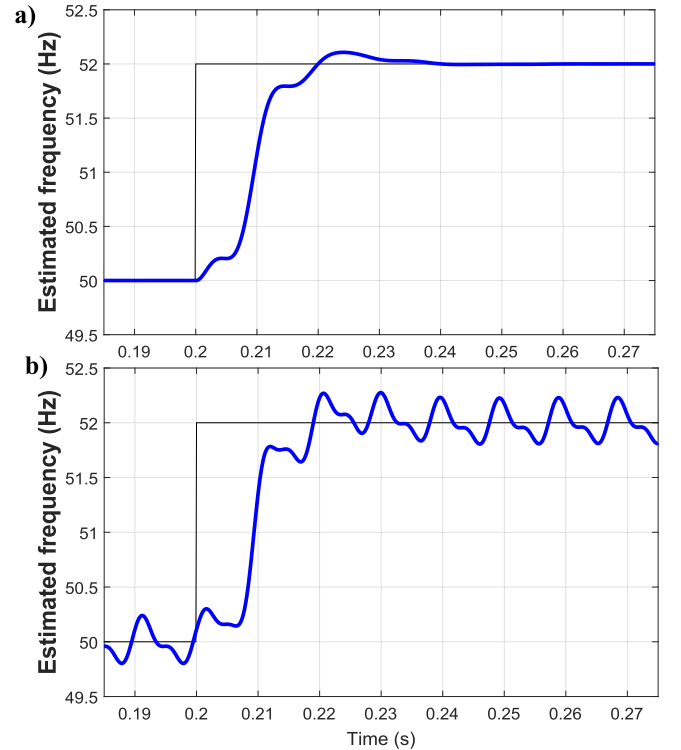

Fig. 13. Transient responses of the SOGI-FLL-E&H to a 2 Hz frequency step perturbation. a) without harmonic distortion. b) with a 3rd harmonic and 3% amplitude voltage regarding nominal.
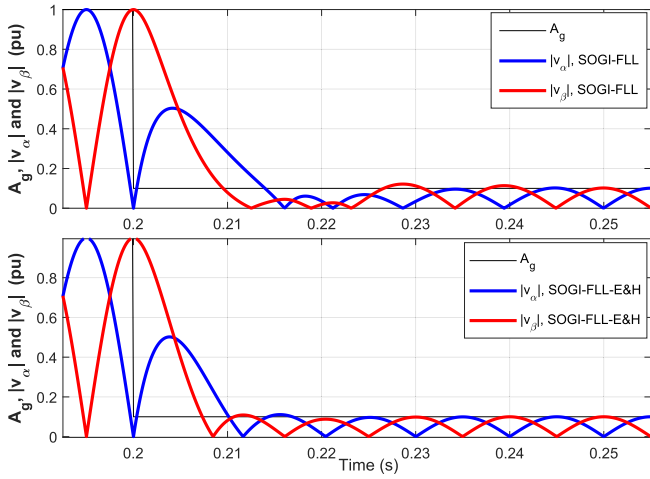
Fig. 14. Grid amplitude voltage, A_g, normalized estimated amplitude voltage, A_{norm}, using eq. (5), in-phase output, v_d, and quadrature-output, v_d, for the SOGI-FLL and SOGI-FLL-E&H, and for a 0.1 pu voltage sag at $t = 0.2s$.
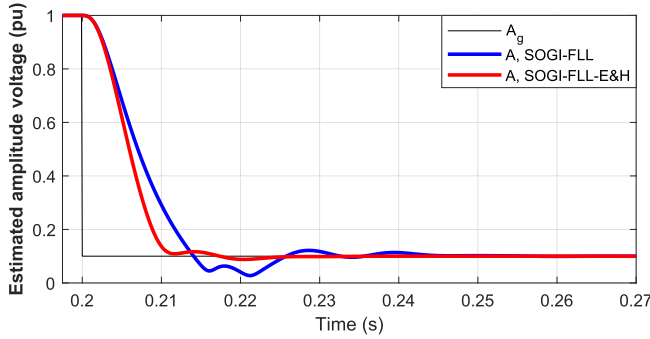

Fig. 15. Grid amplitude voltage, A_g, and estimated amplitude voltage, A, using eq. (4), of the SOGI-FLL and SOGI-FLL-E&H for 0.1 pu voltage sag at $t = 0.2s$.

harmonic distortion. Fig. 13.a depicts the transient response of the SOGI-FLL-E&H for a 2 Hz frequency step change happening at 0.2s. Fig. 13.b shows the same response with a 3rd harmonic with 3% amplitude from nominal. Notice how this threshold allows the SOGI-FLL-E&H to respond to these perturbations without triggering the algorithm.

Fig. 14 depicts the transient responses of the v_α and v_β outputs for both the SOGI-FLL and SOGI-FLL-E&H during a 0.1pu voltage sag happening at $t = 0.2s$. This figure also depicts the fault at the grid amplitude voltage, A_g. Note how the v_α and v_β outputs of the SOGI-FLL-E&H are faster than those of the SOGI-FLL. For the SOGI-FLL-E&H, v_α and v_β arrive to steady state at 0.225s and 0.23s, respectively, while for the SOGI-FLL, they arrive at 0.235s and 0.25s, respectively.

Fig. 15 shows the amplitude voltage estimates obtained by means of eq. (4) of the SOGI-FLL and SOGI-FLL-E&H. It is evident from the figure that the transient response of the estimate A is less distorted in the case of the SOGI-FLL-E&H.

Finally, Figs. 16 and 17 depict the transient responses of the SOGI-FLL and SOGI-FLL-E&H to a short fault transient that consists of a voltage sag (for Fig. 16) and a voltage swell (for Fig. 17), that are returned to nominal values after four periods of the grid voltage. Regarding the moment of the grid voltage at which the fault is being produced, in Fig. 16.a and 17.a the fault happens when the grid is at its maximum voltage, while in Fig. 16.b and 17.b the fault occurs when the grid is at zero voltage.

Regarding the SOGI-FLL in Fig. 16, there are mainly two perturbations: one when the grid voltage drops from 1 pu to 0.2 pu and another when it returns to 1 pu. In the first one, shown in Fig. 16.a, the perturbation arrives at maximum and minimum frequency values of 57.69 Hz and 33.4 Hz, respectively, which correspond to 24.29 Hz peak-to-peak. In the second one, the perturbation reaches at 59.57 Hz and 45.9 Hz, i.e., 13.67 Hz peak-to-peak. On the other hand, for 17.a the measurements of the two perturbations have been measured to be 54.08 Hz and 48.11 Hz for the first perturbation and 45.05 Hz and 52.43 Hz for the second perturbation, respectively, which correspond to 5.97 Hz and 7.38 Hz in peak-to-peak, respectively.

Regarding the SOGI-FLL-E&H, the responses shown in Fig. 16.a and 17.a are flat, while those in Fig. 16.b and 17.b show small and spurious transients, i.e., only when the grid voltage is at zero voltage, as
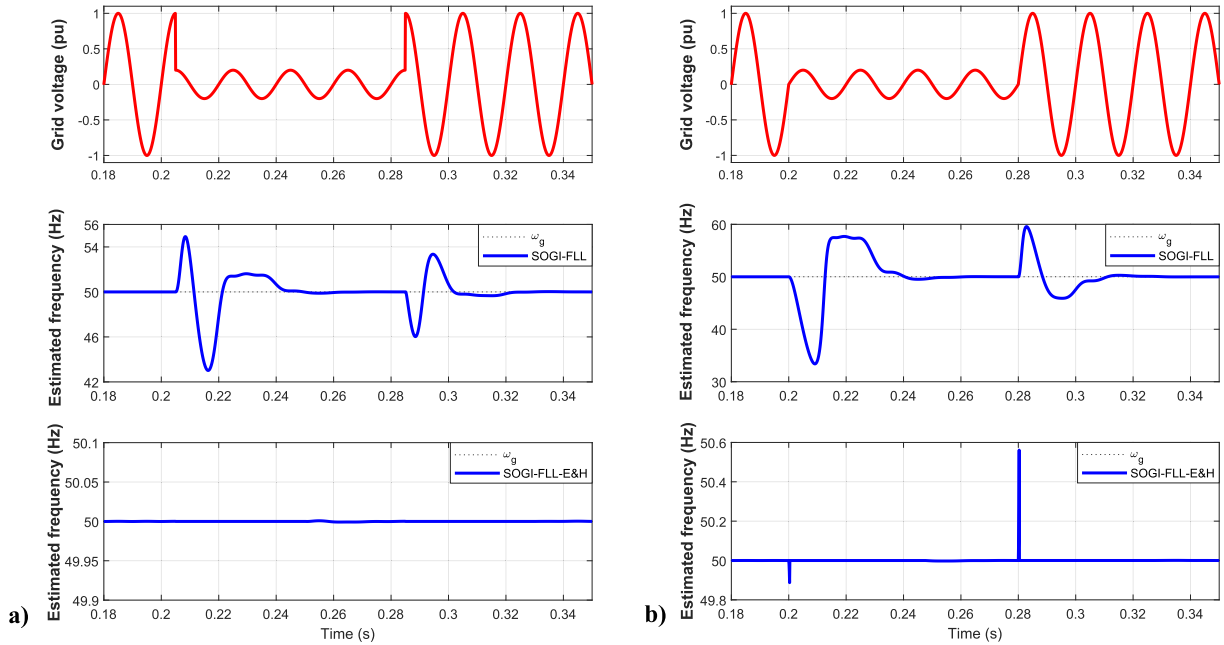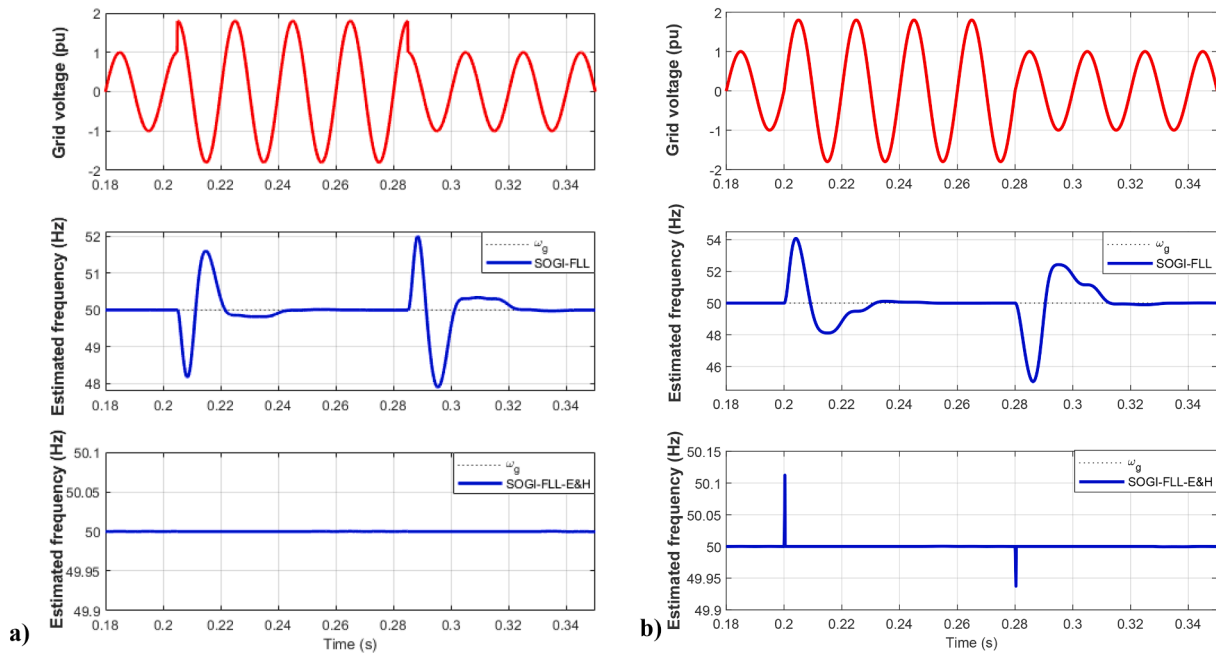

Fig. 16. Transient response of the SOGI-FLL and SOGI-FLL-E&H to a short-duration fault that consists of a voltage sag to 0.2 pu for four periods of the grid and returning afterward to the nominal value. a) Response for the fault happening at the maximum grid voltage level. b) Response to the fault occurring at zero grid voltage level.

Fig. 17. Transient response of the SOGI-FLL and SOGI-FLL-E&H to a short-duration fault that consists of a voltage swell to 1.8 pu for four periods of the grid and returning afterward to the nominal value. a) Response for the fault happening at the maximum grid voltage level. b) Response to the fault occurring at zero grid voltage level.
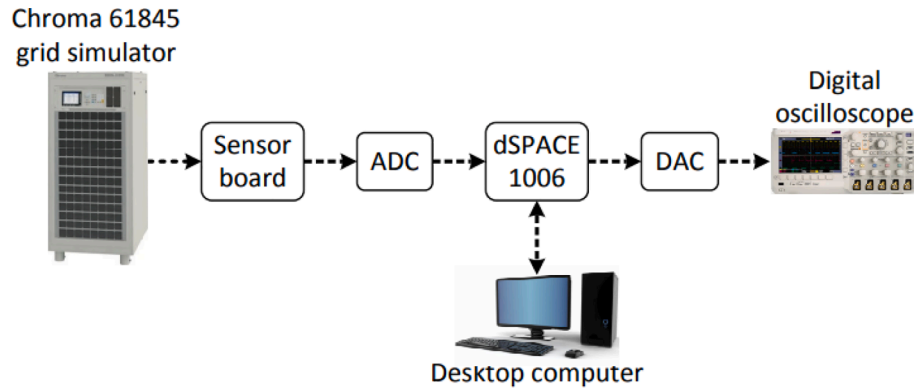

Fig. 18. Experimental setup used to test the SOGI's algorithms.

previously reported, since this is the worst-case scenario. In Fig. 16.b and 17.b, there are two spurious peak transients with peak levels that have been measured and correspond to −0.11 Hz and 0.56 Hz for Fig. 16.b and 0.11 Hz and −0.06 Hz for Fig. 17.b, respectively. Regarding Fig. 16.a and 17.a, simulations have also been performed for other moments of the grid voltage, different from the maximum one, which also show it to be flat. These results are not shown in the paper to limit the extension of the work.

In conclusion, the simulation results demonstrate that the SOGI-FLL-E&H method is capable of handling short faults without showing a noticeable perturbation at the estimated frequency and holding the estimated frequency to the existing one prior to the fault.

The SOGI-FLL and SOGI-FLL-E&H were implemented into a dSPACE 1006 platform with a sampling frequency of 10 kHz. The SOGI's input consists of a single-phase signal taken from a Chroma 61,845 grid simulator with a nominal amplitude voltage of 100 Vrms and a nominal frequency of 50 Hz. This voltage is measured and provided to the dSPACE platform by a sensor board and a DS2004 A/D board; see Fig. 18. The output signals of the SOGI-FLL are then sent out via digital-to-analog converter (DAC) ports and displayed on a Tektronix digital oscilloscope.
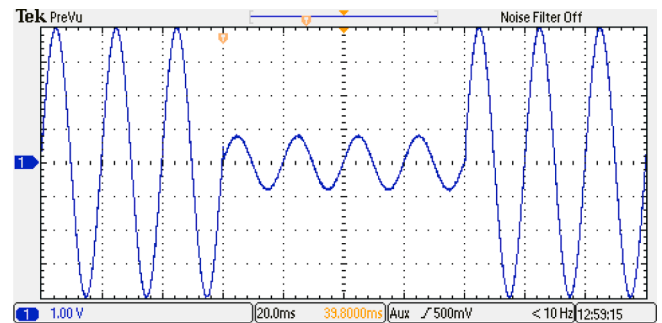

Fig. 19. Experimental short transient fault used for testing the SOGI-FLL and SOGI-FLL-E&H. The transient consists of a sharp change from 1pu to 0.2pu and then back to 1pu. The sag duration is four grid periods. Scope axes: vertical, amplitude voltage (0.25 pu per div); horizontal, time (20 ms per div).

A short transient fault sag of 0.2 pu depth, i.e., from 1 pu to 0.2 pu and then back to 1 pu, identical to the one simulated in Fig. 16, had been tested, with the results shown in Figs. 19, 20, and 21, respectively. The
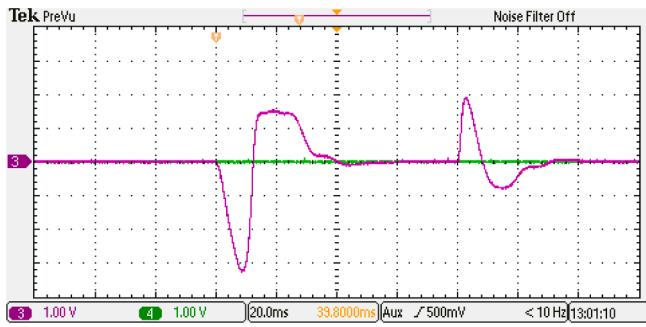
Fig. 20. Experimental transient response of the SOGI-FLL to the short transient fault depicted in Fig. 18. Scope axes: vertical, estimated frequency (5 Hz per div); horizontal, time (20 ms per div).
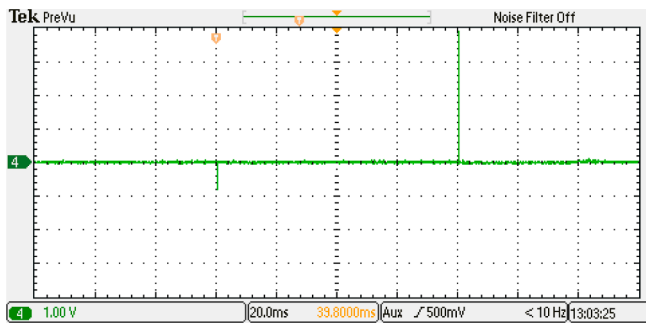

Fig. 23. Experimental transient response of the SOGI-FLL to the short-duration voltage swell of 1.8 pu height. Scope axes: vertical, estimated frequency (2 Hz per div); horizontal, time (20 ms per div).

Fig. 21. Experimental transient response of the SOGI-FLL-E&H to the short transient fault depicted in Fig. 18. Scope axes: vertical, estimated frequency (0.1 Hz per div); horizontal, time (20 ms per div).

Fig. 24. Experimental transient response of the SOGI-FLL-E&H to the short-duration voltage swell of 1.8 pu height. Scope axes: vertical, estimated frequency (0.1 Hz per div); horizontal, time (20 ms per div).

time duration of the transient fault is four periods.

The experimental results in Figs. 20 and 21 are almost identical to the simulated results shown in Fig. 16. Looking at Fig. 20, it can be noticed that the peak-to-peak levels achieved by the SOGI-FLL in the experimental results are very close to the simulated results. In contrast, the experimental results obtained.

with the SOGI-FLL-E&H show a slightly smaller peak-to-peak value compared to the simulated results. Specifically, the measured peak-to-peak values for Fig. 21 are 0.08 Hz and 0.39 Hz, respectively.

A short transient swell of 1.8 pu height, i.e., from 1 pu to 1.8 pu and then back to 1 pu, identical to Fig. 17, had been tested, with the results shown in Figs. 22, 23, and 24. The time duration of the sag fault is four periods.

The results of Figs. 22, 23, and 24 appear to be almost identical to the achieved ones in Fig. 17. Comparing Fig. 23 with Fig. 17.a, the peak levels achieved in the experimental it can be seen that the results are also
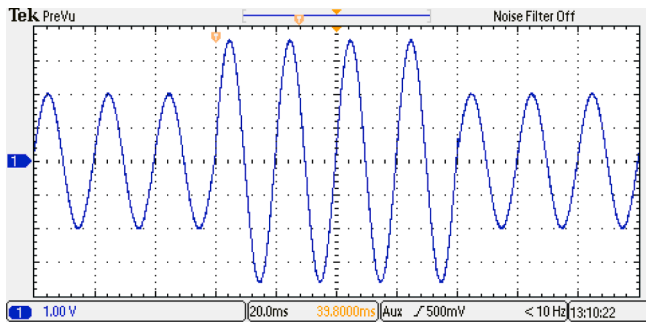
pretty close to the simulated ones. Comparing Fig. 24 with Fig. 17.b, the spurious peak values have been measured to be are 0.11 Hz and −0.06 Hz, which are also close to the simulated ones.

Fig. 25 shows the experimental results for a 2 Hz step change in the grid frequency, and Fig. 26 shows the same response but when the grid has an extra 3rd harmonic with 3% amplitude. Notice that the response, in green, of the SOGI-FLL-E&H is able to accommodate such perturbations, like the simulated ones.

Finally, Fig. 27 shows the experimental result of the SOGI-FLL and SOGI-FLL-E&H amplitude voltage estimates for a 0.1pu voltage sag. Similar to Fig. 15, note that the transient response of the SOGI-FLL-E&H is less distorted than that of the SOGI-FLL.

Fig. 22. Experimental short transient voltage swell fault used to test the SOGI's algorithms. The transient consists of a sharp change from 1pu to 1.8pu and then back to 1pu. The voltage sag duration is four periods. Scope axes: vertical: amplitude voltage (0.5 pu per div); horizontal: time (20 ms per div).
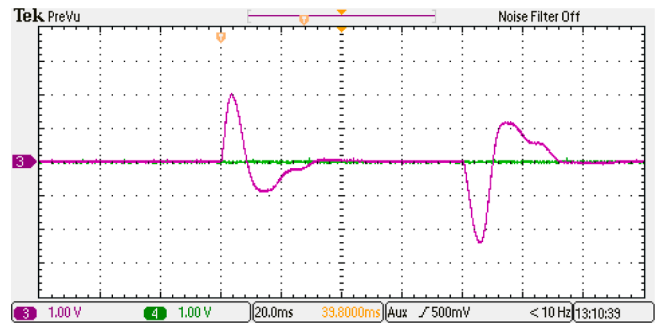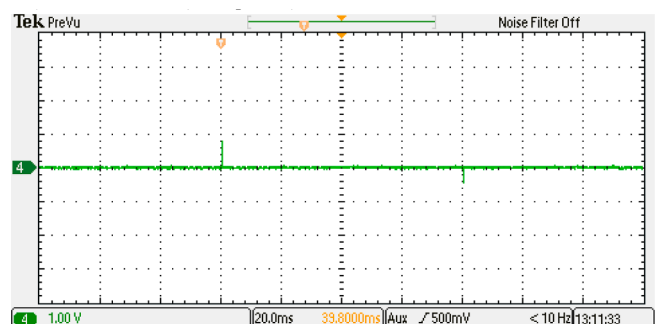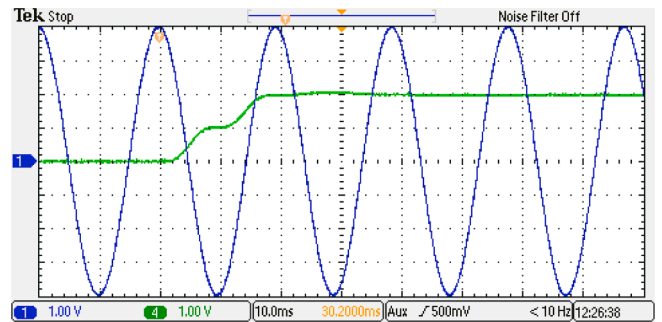

Fig. 25. Experimental transient response of the SOGI-FLL-E&H to a 2 Hz frequency step perturbation of the grid without harmonic distortion. In blue: grid voltage (vertical axe: 0.25pu per div; horizontal axe: 10 ms per div). In green: estimated frequency (vertical axe, 1 Hz per div; horizontal axe, 10 ms per div).
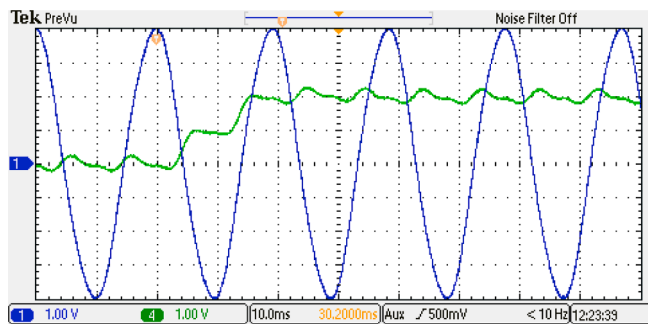
Fig. 26. Experimental transient response of the SOGI-FLL-E&H to a 2 Hz frequency step perturbation with a 3% of 3rd-hamonic in the grid voltage. In blue: grid voltage (vertical axe: 0.25pu per div; horizontal axe: 10 ms per div). In green: estimated frequency (vertical axe: 1 Hz per div; horizontal axe: 10 ms per div).
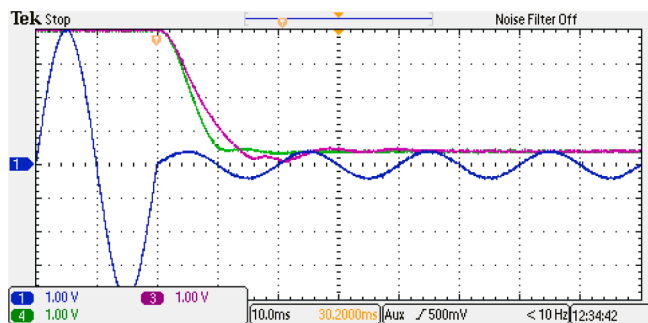

Fig. 27. Experimental transient response of the SOFI-FLL and SOGI-FLL-E&H to a 0.1pu voltage sag. In blue: grid voltage. In green: SOGI-FLL estimated amplitude voltage. In purple: SOGI-FLL-E&H estimated amplitude voltage. Scope axes: vertical (0.25pu per div), horizontal (20 ms per div).

5. Conclusions

This paper proposes an error-and-hold algorithm to improve the performance of the well-known standard SOGI-FLL grid monitoring technique when facing voltage sags and faults. The reason for this is that the estimated FLL frequency response is highly susceptible to these perturbations. To illustrate the extent of the problem, the study uses the LTP model of the SOGI-FLL, which demonstrates how voltage sags and swells affect the amplitude voltage and frequency via an asymmetrical-gain mutual interaction between the SOGI-FLL estimates and a sinusoidal gain that relies on the grid voltage phase. Then, a series of simulations are conducted to reveal the nonlinear and far-reaching impact of voltage sags and swells on the FLL frequency estimate, as well as the impact on the errors induced in the orthogonal outputs of the SOGI.

To mitigate the impact of voltage sags and swells on the estimated FLL frequency and errors induced in the orthogonal outputs of the SOGI, the error-and-hold algorithm utilizes the SOGI's error signal, as well as its absolute and average values, and the average estimated frequency value during these perturbations. The algorithm retains the FLL's estimated frequency at its previous value before the fault and reconstructs the estimated phase during sags and swells perturbations. This allows the SOGI-FLL to provide an estimated frequency and phase without any disturbance during the fault. Once the fault disappears, the estimated frequency and phase return to their normal operation, and the algorithm resumes its standard functionality. To demonstrate the practicality of the proposed algorithm, simulations using MATLAB/Simulink software and experimental results are provided, illustrating how it can enhance the SOGI-FLL's response to these disturbances.

CRediT authorship contribution statement

J. Matas: Conceptualization, Methodology, Software, Validation, Investigation, Writing – original draft, Writing – review & editing. **S. Golestan:** Validation, Writing – review & editing, Supervision. **J. El Mariachet:** Writing – review & editing. **S. Abdali:** Software, Supervision. **W. Al Hanaineh:** Writing – original draft. **J.M. Guerrero:** Supervision.

Declaration of Competing Interest

The authors declare that they have no known competing financial interests or personal relationships that could have appeared to influence the work reported in this paper.

Data availability

No data was used for the research described in the article.

References

[1] IEEE Recommended Practices and Requirements for Harmonic Control in Electric Power Systems, IEEE Std, 1993, 519-1992.
[2] Kusko A, Thompson MC. Power quality in electrical systems. New York, NY, USA: McGraw-Hill; 2007.
[3] Teodorescu R, Liserre M, Rodriguez P. Grid converters for photovoltaic and wind power systems; John Wiley & Sons: Hoboken, Vol. 29; NJ, USA, 2011.
[4] Fuchs E, Masoum M. Power quality in power systems and electrical machines. 2nd ed. Burlington, MA, USA: Elsevier Academic Press; 2015.
[5] Boyra M., Thomas JL. A review on synchronization methods for grid connected three-phase VSC under unbalanced and distorted conditions. In: Proc. of the 14th Eu. Conf. on Pow. Electron. and App., EPE 2011.
[6] Gawhade P, Ojha A. Recent advances in synchronization techniques for grid-tied PV system: A review. Energy Rep 2021;7:6581–99.
[7] Rodríguez P, Luna A, Candela I, Mujal R, Teodorescu R, Blaabjerg F. Multiresonant frequency-locked loop for grid synchronization of power converters under distorted grid conditions. IEEE Trans Ind Electron 2011;58:127–38.
[8] Gude S, Chu C-C. Three-phase PLLs by using frequency adaptive multiple delayed signal cancellation prefilters under adverse grid conditions. IEEE Trans on Ind App 2018;54(4):3832–44.
[9] Ma W, Ouyang S, Xu W. Improved frequency locked loop based synchronization method for Three-Phase Grid-Connected Inverter under Unbalanced and Distorted Grid Conditions. Energies 2019;12:1023.
[10] Yu J, Yang B, Zhu P, Zhang L, Peng Y, Zhou X. An improved digital phase locked loop against adverse grid conditions. Energy Rep 2022;8:714–23.
[11] Karimi-Ghartemani M, Khajehoddin SA, Jain PK, Bakhshai A, Mojiri M. Addressing DC component in PLL and notch filter algorithms filter algorithms. IEEE Trans Power Electron, Jan 2012;27(1):78–86.
[12] Matas J, Castilla M, Miret J, Garcia de Vicuna L, Guzman R. An adaptive prefiltering method to improve the speed/accuracy tradeoff of voltage sequence detection methods under adverse grid conditions. IEEE Trans Ind Electron 2014;61(5):2139–51.
[13] Hui N, Wang D, Li Y. An efficient hybrid filter-based phase-locked loop under adverse grid conditions. Energies 2018;11:703.
[14] Hui N, Feng Y, Han X. Design of a high performance phase-locked loop with DC offset rejection capability under adverse grid condition. IEEE Access 2020;8: 6827–38.
[15] Smadi IA, Kreashan HA, Atawi IE. Enhancing the filtering capability and the dynamic performance of a third-order phase-locked loop under distorted grid conditions. Energies 2023, 16, 1472.
[16] Cao Y, Yu J, Xu Y, Li Y, Yu J. An efficient phase-locked loop for distorted three-phase systems. Energies 2017;10:280.
[17] Matas J, Martín H, De La Hoz J, Abusorrah A, Al-Turki YA, Alshaeikh HA. New THD measurement method with small computational burden using a SOGI-FLL grid monitoring system. IEEE Trans Power Electron 2020;35:5797–811.
[18] Abdali Nejad S, Matas J, Martín H, de la Hoz J, Al-Turki YA. New SOGI-FLL grid frequency monitoring with a finite state machine approach for better response in the face of voltage sag and swell faults. Electronics 2020;9(4):612.
[19] Abdali Nejad S, Matas J, Elmariachet J, Martín H, de la Hoz J. SOGI-FLL grid frequency monitoring with an error-based algorithm for a better response in face of voltage sag and swell faults. Electronics 2021;10(12):1414.
[20] Gulipalli SC, Gude S, Peng SC, Chu CC. Multiple delayed signal cancellation filter-based enhanced frequency-locked loop under adverse grid conditions. IEEE Trans on Ind App 2022;58(5):6612–28.

[21] Matas J, Martin H, de la Hoz J, Abusorrah A, Al-Turki YA, Al-Hindawi M. A family of gradient descent grid frequency estimators for the SOGI filter. IEEE Trans Power Electron 2018;33:5796–810.

[22] Golestan S, Ebrahimzadeh E, Guerrero JM, Vasquez JC. An adaptive resonant regulator for single-phase grid-tied VSCs. IEEE Trans Power Electron 2018;33: 1867–73.

[23] Matas J, Martín H, ElMariachet J, Abusorrah A, Al-Turki YA. A new LPF-based grid frequency estimation for the SOGI filter with improved harmonic rejection. In Renewable Energy and Power Quality Journal (RE&PQJ); UPCommons: Salamanca, Spain; 2018.

[24] Golestan S, Guerrero JM, Vasquez JC, Abusorrah AM, Al-Turki Y. Modeling, Tuning, and performance comparison of second-order-generalized-integrator-based FLLs. IEEE Trans Power Electron 2018;33:10229–39.

[25] Du H, Sun Q, Cheng Q, Ma D, Wang X. An adaptive frequency phase-locked loop based on a third order generalized integrator. Energies 2019;12:309.

[26] Golestan S, Guerrero JM, Vasquez JC. Modeling and stability assessment of single-phase grid synchronization techniques: Linear time periodic versus linear time-invariant frameworks. IEEE Trans Power Electron, Jan 2019;34(1):20–7.

[27] Golestan S, Guerrero JM, Musavi F, Vasquez JC. Single-phase frequency-locked loops: a comprehensive review. IEEE Trans Power Electron 2019;34:11791–812.

[28] Golestan S, Guerrero JM, Vasquez JC, Abusorrah AM, Al-Turki Y. Standard SOGI-FLL and its close variants: precise modeling in LTP framework and determining stability region/robustness metrics. IEEE Trans Power Electron 2021;36:409–22.